Applied Acoustics 82 (2014) 6–14

Contents lists available at ScienceDirect

Applied Acoustics

journal homepage: www.elsevier.com/locate/apacoust

Source excitation strategies for obtaining impulse responses in finite difference time domain room acoustics simulation

Damian T. Murphy [a,*], Alex Southern [b], Lauri Savioja [b]

[a] AudioLab, Department of Electronics, University of York, York, UK
[b] Department of Media Technology, Aalto University School of Science, Espoo, Finland

ARTICLE INFO

Article history:
Received 13 April 2012
Received in revised form 20 February 2014
Accepted 24 February 2014
Available online 25 March 2014

Keywords:
Room acoustic simulation
Finite difference scheme

ABSTRACT

This paper considers source excitation strategies in finite difference time domain room acoustics simulations for auralization purposes. We demonstrate that FDTD simulations can be conducted to obtain impulse responses based on unit impulse excitation, this being the shortest, simplest and most efficiently implemented signal that might be applied. Single, rather than double, precision accuracy simulations might be implemented where memory use is critical but the consequence is a remarkably increased noise floor. Hard source excitation introduces a discontinuity in the simulated acoustic field resulting in a shift of resonant modes from expected values. Additive sources do not introduce such discontinuities, but instead result in a broadband offset across the frequency spectrum. Transparent sources address both of these issues and with unit impulse excitation the calculation of the compensation filters required to implement transparency is also simplified. However, both transparent and additive source excitation demonstrate solution growth problems for a bounded space. Any of these approaches might be used if the consequences are understood and compensated for, however, for room acoustics simulation the hard source is the least favorable due to the fundamental changes it imparts on the underlying geometry. These methods are further tested through the implementation of a directional sound source based on multiple omnidirectional point sources.

1. Introduction

The finite difference time domain method (FDTD) is a discrete spatio-temporal numerical simulation method that has been shown as being appropriate for modeling acoustic wave propagation in an enclosed system [1,2,3]. Recent developments in frequency dependent absorbing and diffusing boundaries [4,5] offer the potential for a more complete approach to room acoustics simulation. However, full audio bandwidth simulations for even a small room of any acoustic interest are very demanding in terms of both computation time and required memory, and so these techniques are often best used for low-frequency simulation only. The consequence of these computational requirements being that work in this area has usually relied on offline computation of the impulse response (IR) for a given space and source/receiver combination. This IR can then readily be used in a real-time audio convolution scheme suitable for auralization purposes. In addition, these results can be applied to any type of room acoustic analysis that is based on deriving parameters from a suitable IR, including computation of typical room acoustic metrics, such as reverberation time (T_{30}), or clarity ($C_{50/80}$). However, for some other purposes, such as visualization of the sound field, calculation of the whole field based on some form of smoothed excitation signal applied over a longer duration might be a more suitable approach.

Generally, in such room acoustic simulations, a sound source is considered as a time-varying pressure signal applied to a single point on the FDTD grid. A receiver is defined as any other grid point where the numerical response to this source signal is measured, and for auralization purposes, receivers may be grouped individually (mono), as a pair (stereo), or as an array of points (multi-channel surround-sound). In this way, the signal observed at the receiver is analogous to a measurement microphone that acts as a scalar sensor of sound pressure. Based on this concept, in order to obtain an IR, the sound source should ideally propagate omnidirectionally and demonstrate a flat frequency response over a defined bandwidth. To this end, different source signals have been proposed in the literature enabling appropriate control over this required bandwidth (see e.g. [6,7]), with single-point source direc-

* Corresponding author. Tel.: +44 1904323221.
E-mail addresses: damian.murphy@york.ac.uk (D.T. Murphy), alex.southern@aalto.fi (A. Southern), lauri.savioja@aalto.fi (L. Savioja).

http://dx.doi.org/10.1016/j.apacoust.2014.02.010
0003-682X/

tionality dependent on the propagation characteristics of the FDTD grid itself. Typically however, although usually defined in terms of sound pressure, the discrete-time excitation signal itself can take any form such that it is sampled commensurate with the sampling rate of the FDTD grid used (see e.g. [8]).

The application and implementation of such a defined pressure-like signal has been characterized in [10], either as a *hard source*, *additive source*, also known as a *soft source* [11], or *transparent source*. Each of these source types, hard, soft and transparent, differ in terms of their relative advantages and disadvantages. With a hard source, the pressure at the source grid point is determined by the driving excitation function alone, ideally coupling the signal into the grid, making them the simplest and easiest to implement. However, in doing this they disregard the underlying grid function, and for certain signals, this discontinuity between source function and grid function results in large, low frequency pressure ripples that can be observed at all other grid points [11]. In addition to having little correlation with actual physical sound sources, hard sources also act as signal scatterers for any incident wave. As a consequence they become a discontinuity or perturbation in the medium, or can be considered as a sound radiating, perfectly reflecting boundary node with a size corresponding to the spatial sampling interval [6].

With a soft source, the driving excitation function is added (hence also *additive* source) to the numerical pressure value at the source grid point. The implementation is no more difficult than with a hard source, with the added advantage of no perturbation being added to the problem domain, and hence no additional numerical artefacts or reflected components. In this case, the disadvantage is that the pressure function at the source grid point no longer resembles the applied excitation function. Ideally, as recommended in [11], the response should be measured at the source grid point and used to normalize the output at other grid points, with the suggestion that this is the reason why soft source excitation has not been extensively used in the acoustics literature. In addition, soft sources exhibit solution growth due to source–boundary interaction effects [6], requiring further pre-or post-simulation conditioning to obtain a useful IR, e.g. differentiation of the original pressure-based signal [6], or pre-filtering [8].

A transparent source, as defined in [10] is one that propagates the same signal as a hard source, but does not act as a signal scatterer (it is *transparent* to an incident wave). It therefore offers the benefits of a hard source in terms of how it couples the excitation signal into grid, but does not result in a perturbation in the problem domain. The disadvantage with such a source being that a compensation filter, required to remove the effect of the fixed grid point, must be computed prior to simulation, and that the excitation function itself becomes more complex – and computationally demanding – to implement.

This paper contains several practical results that affect how FDTD simulations should be conducted with a special emphasis on these three excitation types. We also note that these different source models have different physical interpretations (see e.g. [6,7]) with different practical consequences as a result, and it is this latter point that is the focus of this paper. First, we demonstrate that a unit impulse is sufficient and good choice for an excitation signal, especially with double precision accuracy (Section 2). Similarly, we show by numerical examples that a hard source introduces error in detected modes, soft sources cause an offset in the received level, while a transparent source performs without these artefacts, thus making it an attractive choice (Section 3). Finally, we demonstrate that hard sources have serious problems if they are to be used to create directive sources, instead, soft and transparent sources behave in an ideal manner and reproduce the directivity patterns as expected (Section 4).

2. The finite difference time domain method in room acoustics simulation

There are basically two different FDTD formulations applied in room acoustic simulation: the vector wave equation based model that considers both sound pressure and particle velocity [11], and the scalar wave equation based model that uses only sound pressure [5]. However, they are equivalent in terms of the results they produce, and in this work we use the scalar wave equation model as it is computationally more efficient [9]. The following describes this FDTD method for the 3-D acoustic wave equation:

$$p^{n+1}_{i,j,k} = \lambda^2\left(p^n_{i+1,j,k} + p^n_{i-1,j,k} + p^n_{i,j+1,k} + p^n_{i,j-1,k} + p^n_{i,j,k+1} + p^n_{i,j,k-1}\right) + 3(1-3\lambda^2)p^n_{i,j,k} - p^{n-1}_{i,j,k} \quad (1)$$

The 2-D case is given by:

$$p^{n+1}_{i,j} = \lambda^2\left(p^n_{i+1,j} + p^n_{i-1,j} + p^n_{i,j+1} + p^n_{i,j-1}\right) + 2(1-2\lambda^2)p^n_{i,j} - p^{n-1}_{i,j} \quad (2)$$

where i,j and k denote spatial indices, p^n is the pressure value at time-step n and λ is the Courant number, which is usually set to the limiting value such that for the 3-D case $\lambda = \frac{1}{\sqrt{3}}$, and for the 2-D case $\lambda = \frac{1}{\sqrt{2}}$ thereby simplifying the above expressions further. This approach results in a rectilinear spatio-temporal sampling of connected nodes across the problem space. Boundary conditions are dealt with separately, and can be defined with parameters that determine both frequency dependent absorption [4] and diffusion characteristics [5]. The grid sampling rate f_{update} is related to the spatial sampling distance d according to $f_{update} = \frac{c\sqrt{2}}{d}$ where c is the speed of sound.

It is worth noting that this simple scheme suffers from direction dependent dispersion error, the effects of which can be improved upon by using more advanced schemes with a larger stencil [12,13]. However, we consider this scheme general enough to be applied here with any exceptions to this assumption explicitly noted in the text.

3. Source excitation

A number of methods for applying source excitation have been explored in FDTD and related literature for room acoustics simulation. The aim of any such simulation is to obtain the impulse response $h(n)$ of the system consisting of a (generally) enclosed geometry together with a given source/receiver combination and hence the unit impulse is the ideal source excitation input.

3.1. Choice of source signal and finite precision variable considerations

In real room acoustic measurement a specific analytic excitation signal is used to obtain the impulse response of the space given that a perfect impulse cannot be applied. In FDTD simulations a similar approach is adopted through the use of an appropriate time varying source function (see e.g. [11] for a recent summary) noting that for non-impulse like excitation, the time varying input signal should also be deconvolved from the output to obtain the impulse response. Given that the FDTD equations are linear and time-invariant, as are the three given source types, it is therefore possible to use convolution to obtain the output for any given input signal based only on the measured impulse response. The advantage here being that the unit impulse is the simplest to apply and also the shortest – and hence most efficient in terms of reducing overall simulation run-time, especially when compared to using longer form analytical signals (e.g. exponential sine sweep as commonly used in room acoustic measurement) or direct excitation with an anechoic audio signal. If some other excitation is required, it can be applied post simulation by convolving the desired

excitation signal with the obtained impulse response. By way of example, Fig. 1a shows a waterfall plot of one simulation, where a Hanning windowed 9-cycle sine wave excitation at 500 Hz was applied to a 2-D FDTD grid having f_{update} = 44,100 Hz, resulting in a 1000 sample output. The waterfall plots have been produced using a 2048-point FFT and a sliding 128-point Hamming window with an overlap value of 0.75. The receiver was located 2 m away from the sound source in the diagonal direction with respect to the grid, along which numerical dispersion effects are minimized for the direct sound path considered in this example relative to other wave propagation directions. This test case was compared to a simulation in which the 1000-point impulse response was computed first and then convolved with the 500 Hz sine wave applied in the first test. The difference between these two is illustrated in Fig. 1b. The observed difference is minimal and caused by the effects of finite precision accuracy. The same result can be found at all frequencies and for all source types (hard, soft, transparent).

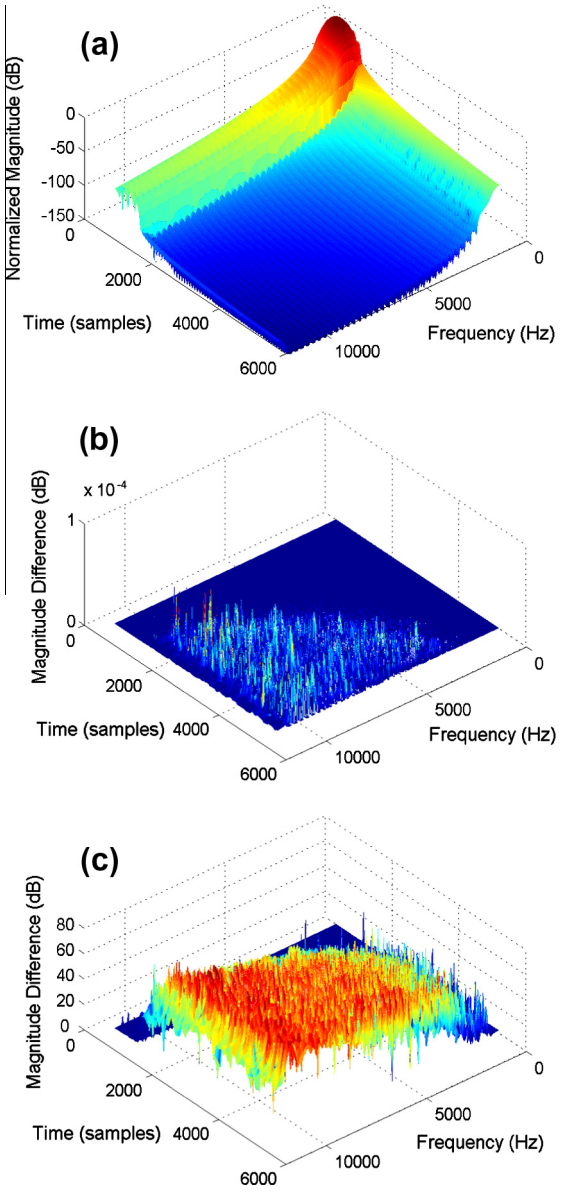

Fig. 1. Time–frequency observations of directly applied signal excitation compared with impulse response measurement and convolution (a) Hanning windowed 500 Hz 9-cycle sine wave excitation applied to a 2-D FDTD grid measured 2 m from the excitation point in the diagonal direction; (b) the difference between the example shown in (a) and the same case obtained via impulse response measurement and convolution; (c) the same result obtained using single- rather than double-precision accuracy calculations.

Finite precision numerical effects become a more critical factor when using single-precision floating-point numbers for storing and calculating pressure values p^n as might be typical with an FDTD GPU based implementation, see e.g. [14–17]. The example in Fig. 1a was carried out with double-precision accuracy and the same test is repeated at single-precision. Fig. 1c shows the difference between direct simulation and simulation via convolution as before, but now based on results obtained using single-precision accuracy. As can be seen, there is a significant increase in the overall noise level (of the order of 60 dB peak values), as would be expected, due to the reduced dynamic range of the system. The useful signal-to-noise ratio remains of the order of 90 dB. The implication being that single-precision accuracy should be avoided where possible but with double-precision accuracy an impulse excitation is sufficient for any purpose, and in particular for convolution based auralization where the effects of an increased noise floor level can become audible.

3.2. Source type

Consider the 3-D case, with $\lambda = \frac{1}{\sqrt{3}}$, noting that the 2-D case follows trivially. Let p^n_{in} be defined as an arbitrary input signal at time-step n applied at grid point (u, v, w). Then (1) is redefined at this point for each source type as follows:

$$p^{n+1}_{(u,v,w),hard} = p^{n+1}_{in} \tag{3}$$

$$p^{n+1}_{(u,v,w),soft} = \frac{1}{3}\left(p^n_{u+1,v,w} + p^n_{u-1,v,w} + p^n_{u,v+1,w} + p^n_{u,v-1,w} + p^n_{u,v,w+1} + p^n_{u,v,w-1}\right) - p^{n-1}_{u,v,w} + p^{n+1}_{in} \tag{4}$$

where $p^{n+1}_{(u,v,1),hard}$ and $p^{n+1}_{(u,v,w),soft}$ are respectively the new grid update equations for a hard or soft source excitation at grid point (u, v, w). Hence (3) is simply the input function applied directly at this point, replacing the standard update Eq. (1), and (4) is the input function superimposed or added to the standard update Eq. (1). However, the update equation for a transparent source $p^{n+1}_{(u,v,w),trans}$ is less obvious, as follows:

$$p^{n+1}_{(u,v,w),trans} = \frac{1}{3}\left(p^n_{u+1,v,w} + p^n_{u-1,v,w} + p^n_{u,v+1,w} + p^n_{u,v-1,w} + p^n_{u,v,w+1} + p^n_{u,v,w-1}\right) - p^{n-1}_{u,v,w} + p^{n+1}_{in} - \sum_{t=0}^{n} h^{n-t+1}_{3D} p^t_{in} \tag{5}$$

where, in this case, h^n_{3D} is defined as the impulse response of the 3-D FDTD mesh at the point of excitation, when the input is applied as a hard source such that:

$$p^n_{in} = \begin{cases} 1 & \text{for } n = 0 \\ 0 & \text{for } n \neq 0 \end{cases} \tag{6}$$

A transparent source therefore subtracts the value of the convolution of the input signal p^n_{in} and the mesh impulse response $h^n_{3D/2D}$ from the source grid point. This ensures that the value of the excitation function applied at the source point is equivalent to a directly applied hard source but with the additional reflections that result in this particular situation effectively canceled out. Note that this formulation of transparent source excitation is a modification of that considered in [10], this being for the scalar, single variable FDTD implementation of the wave equation, as commonly used in room acoustics simulation problems. Note also that this method of transparent source excitation can also be used for other FDTD stencils/implementations with an appropriate reformulation of (5) and calculation of the grid specific compensation signal h^n_{3D}.

3.3. Obtaining the compensation signal

The mesh impulse response, $h^n_{3D/2D}$, at the point of excitation can be obtained in a number of ways. A hard source excitation is applied as in (3) such that p^n_{in} is defined as in (6). For a source applied at 3-D grid point (u, v, w) h^n_{3D} is therefore obtained as follows:

$$h^n_{3D} = \frac{1}{3}\left(p^{n-1}_{u+1,v,w} + p^{n-1}_{u-1,v,w} + p^{n-1}_{u,v+1,w} + p^{n-1}_{u,v-1,w} + p^{n-1}_{u,v,w+1} + p^{n-1}_{u,v,w-1}\right) - p^{n-2}_{u,v,w} \tag{7}$$

Hence h^n_{3D} is the measured output at the point of excitation, defined as a hard impulsive source, using the standard update Eq. (1) only – note that the excitation function is decoupled from the FDTD grid as the measured output at this point has no influence on the input. The input is defined only by the unit impulse excitation function [10].

The most straightforward method of obtaining h^n_{3D} is to define a grid geometry sufficiently large to ensure there are no reflected components incident on the excitation point (u, v, w), and such that n is greater than the length of the room impulse response required from any subsequent simulation. Although this may be problematic to compute for sufficient n, especially for the 3-D case, it only has to be done once and $h^n_{3D/2D}$ can then be stored for use in any simulation where the length of the required IR in samples is less than n. If it is not possible to obtain $h^n_{3D/2D}$ for values of n where the large geometry required prohibits efficient implementation, symmetry in 2-D or 3-D can be exploited to compute $h^n_{3D/2D}$ over a much reduced grid size [10]. For instance, a 2-D square grid has four axes of symmetry and the entire grid can be simulated by computing only the grid points bounded by the triangle formed by Cartesian axes, $y = 0,\ x = y,\ x = n/2$, such that the entire mesh is of dimension (n, n), with (u, v, w) located at the center point origin of this grid coordinate system. This reduces the required computational domain to $1/8$ of the total grid size. The rotational symmetry of a 3-D cube can be exploited similarly to reduce the required computational domain to $1/24$ of the total grid size. Both offer significant savings in memory and computation time allowing much longer compensation signals to be computed with even modest computing power.

For sufficiently large n it is also possible to approximate $h^n_{3D/2D}$, as it slowly tends to zero. Alternatively, an analytical solution that might be used for obtaining h^n_{2D} has been presented [18]. Fig. 2a illustrates the first part of h^n_{2D} calculated up to $n = 5100$ timesteps using a 5100×5100 rectilinear grid. In the 3-D case h^n_{3D} has been calculated up to $n = 1000$ timesteps, and is shown for up to $n = 100$ in Fig. 2c. Note that h^n_{3D} converges more rapidly to zero than h^n_{2D}, justifying the shorter calculation length.

4. Comparison of source excitation methods

Three test cases are used to explore the practical application of hard, soft and transparent unit impulse source excitation. The first considers a simple bounded 3-D geometry and presents the impulse responses obtained under each excitation. The second case considers the modal frequencies that emerge in a 2-D bounded structure, and the third applies these techniques in a typical auralization application, where it is required to simulate the characteristics of a directional source.

4.1. Impulse responses obtained from simulation

This test case is designed to obtain and evaluate the impulse responses obtained under hard, soft and transparent unit impulse source excitation for a typical bounded space. The space in question is a cuboid room of dimension $3 \times 5 \times 2$ m. The source is placed at (0.9, 0.9, 0.9) and the receiver p_{out} at (2.1, 4.1, 1.1), the opposite corner through the elevated diagonal. $f_{update} = 30$ kHz, and all boundaries are set to be almost totally reflecting with reflection coefficient $r = 0.999$. The simulations are run for 60,000 timesteps, sufficient to obtain 2 s impulse responses and the results are presented in Figs. 3 and 4.

Fig. 3a–c show the impulse responses $p_{out,hard}$, $p_{out,soft}$ and $p_{out,transparent}$ respectively with their corresponding frequency response plots. Note that in each case the gray plot is the raw output from the simulation, and the black plot is the same data filtered for DC. Both soft and transparent sources demonstrate an increasing DC-offset at the output, as expected given the nature of their excitation and the discussion presented in Section 1.

Fig. 4a and b plot the differences $p_{out,transparent} - p_{out,hard}$ and $p_{out,transparent} - p_{out,soft}$ respectively with their corresponding frequency response plots. In these examples the data has already been filtered for DC. It can be observed that the soft source excitation adds a broadband offset to the overall response that is not present in the hard or transparent source cases.

4.2. Modal analysis

Transparent source excitation is stated as being the optimal method of obtaining the system response to a given excitation without introducing numerical artefacts caused by hard or soft approaches [10,11]. In particular [10] explored how transparent excitation removes the additional reflected components caused by wavefronts incident on a hard source position that has been implemented by fixing a grid point to a specific value. This issue potentially becomes more critical in a bounded geometry, as used in a typical room simulation, where there are many reflections that re-

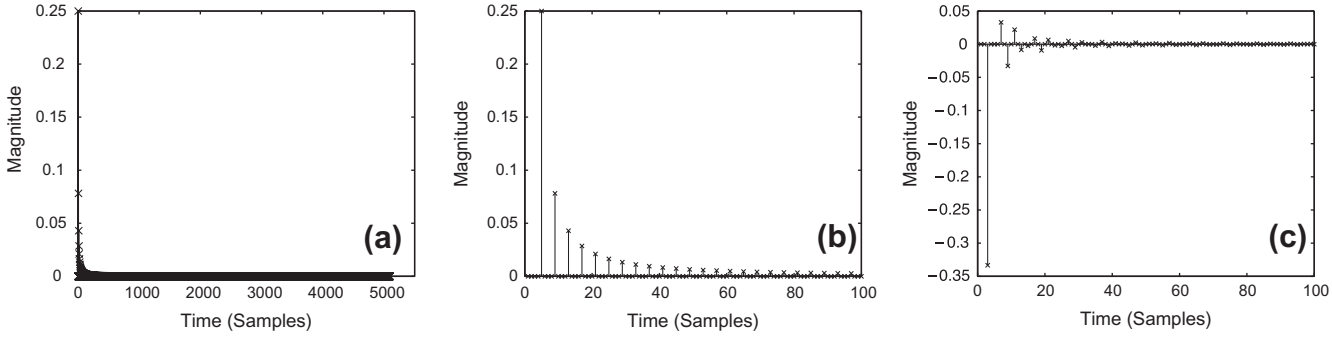

Fig. 2. Transparent source compensation signals: (a) h^n_{2D} calculated up to $n = 5100$ timesteps; (b) a close up of the first 100 timesteps, noting that only every fourth sample is non-zero and that the signal rapidly converges to zero even after 100 timesteps; (c) h^n_{3D} calculated up to $n = 1000$ and shown for $n = 100$ timesteps, noting that only every second sample is non-zero and that the signal converges more rapidly to zero than the 2-D case.

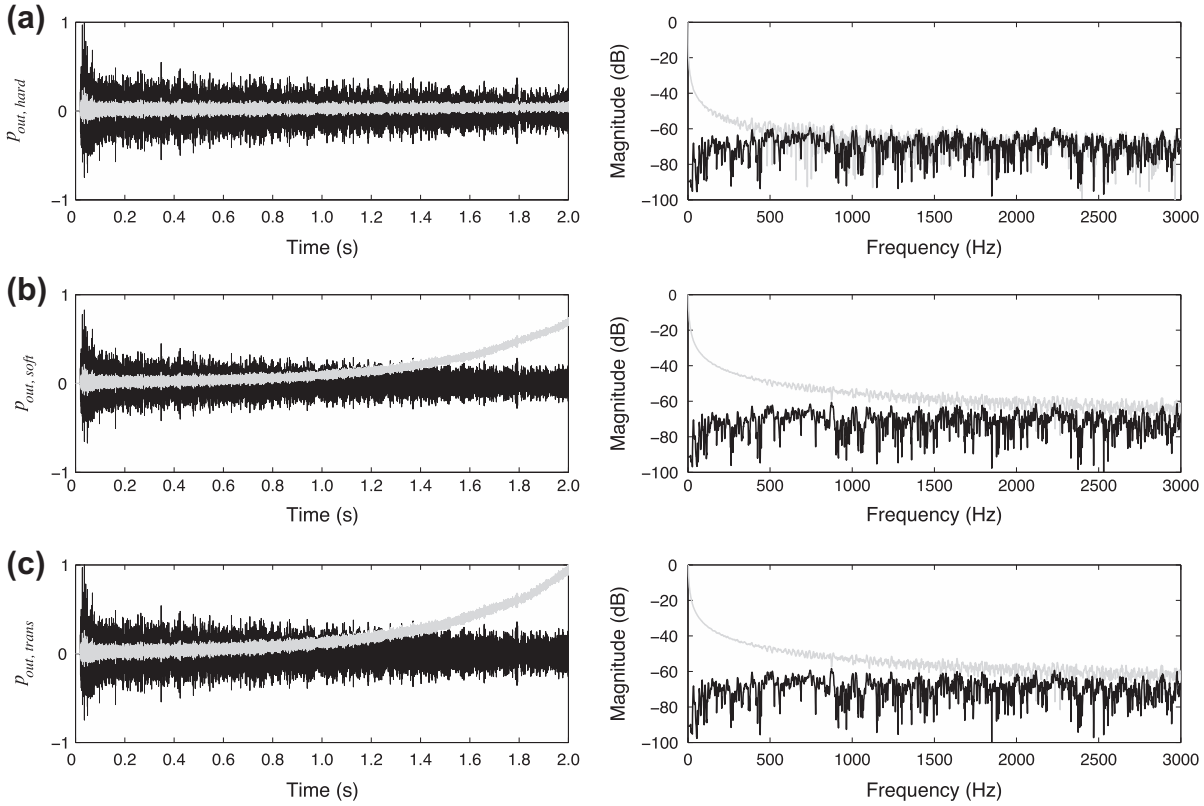

Fig. 3. Simulation results obtained from a $3 \times 5 \times 2$ m room with almost totally reflecting boundaries. (a) Impulse response (left) and frequency response (right) under hard source excitation; (b) impulse response and frequency response under soft source excitation; (c) impulse response and frequency response under transparent source excitation. In each case the gray plot represents the raw output from the simulation with the black plot showing the same after filtering for DC.

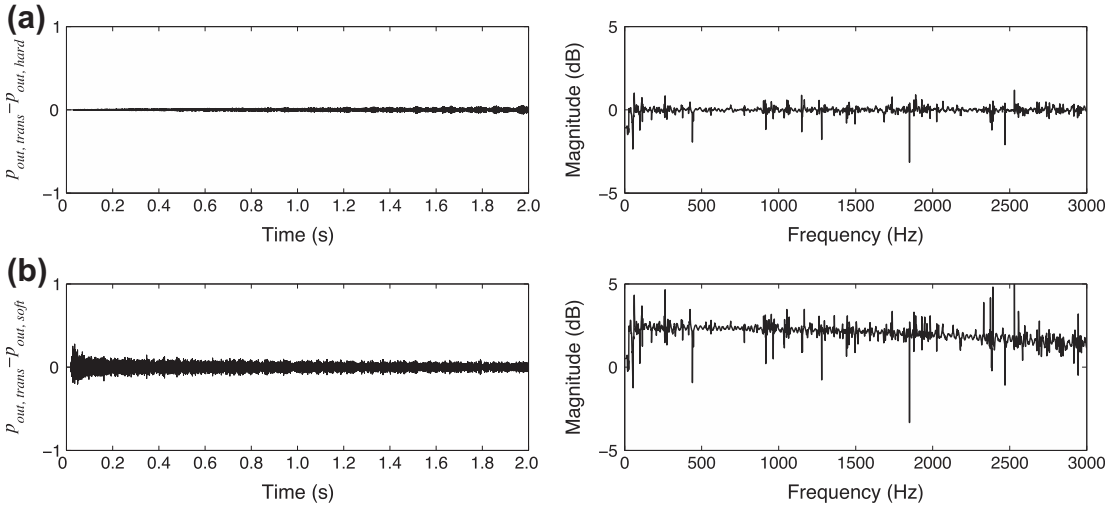

Fig. 4. (a) The difference between impulse responses obtained under transparent and hard source excitation (left) and the corresponding frequency response (right). (b) The difference between impulse responses obtained under transparent and soft source excitation (left) and the corresponding frequency response (right), noting the offset that has been added due to the soft source case. DC removal has been applied in all results presented.

sult in a complex and diffuse soundfield. The following test explores the implication of these source excitation methods on the modal frequencies observed from the associated impulse response.

A 5×5 m 2-D space is defined with the source initially located at (0.5, 2.0) and receivers at (3.0, 4.5), (3.5, 4.0), (4.0, 3.5), and (4.5, 3.0), using a rectilinear grid with coordinate origin located at the bottom left hand corner such that $f_{update} = 44{,}100$ Hz. Boundaries are set to be totally reflecting and an IR is obtained at the receiver points under soft, hard and transparent source excitation. The magnitude response of each is obtained via an FFT, normalized with respect to the largest peak obtained across all three measurements and the results up to 160 Hz (for clarity) are presented in Fig. 5a for output point (4.5, 3.0). Noting that the magnitude response is only considered up to 160 Hz, and that $f_{update} = 44{,}100$ Hz, dispersion error effects can be discounted in the results which follow. Note also that the input and output points all lie along the

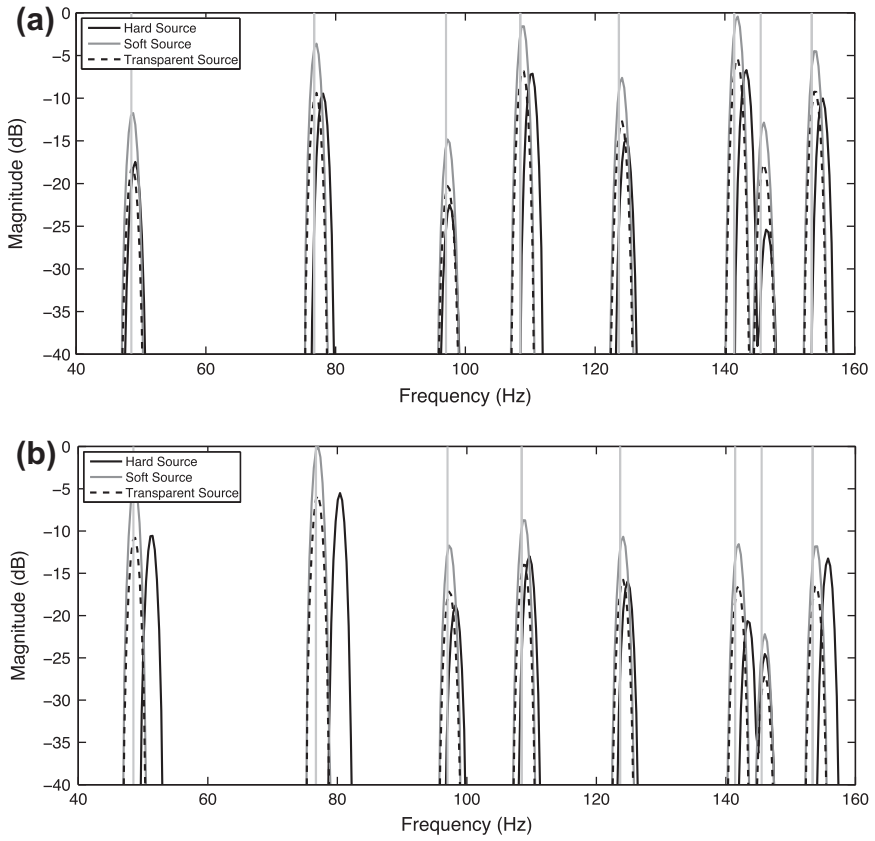

Fig. 5. The modal response of a 2-D 5 × 5 m rectilinear grid under hard (black solid line), soft (gray solid line) and transparent (black dashed line) source excitation. Overlaid are the first eight analytical modes. (a) Input point (0.5, 2.0), output point (4.5, 3.0); (b) input point (1.5, 2.0), output point (4.5, 3.0). Note that with the hard source, the fixed grid point results in a shifting of the expected resonant frequencies, dependent on input position, whereas there is agreement in terms of frequency for both soft and transparent cases.

closed square path aligned with the grid diagonals associated with the wavevectors that will result in the modal series $f_{(x,y)}$ as defined by:

$$f_{(x,y)} = \frac{c}{2}\sqrt{\left(\frac{x}{L_x}\right)^2 + \left(\frac{y}{L_y}\right)^2} \tag{8}$$

where in this case $L_x = L_y = 5$ m. The first eight individually identifiable analytical modes for a 2-D space of this particular geometry are also obtained using (8) and are plotted as vertical lines overlaid on the frequency response plot. For clarity, the peak values and relative magnitude values are presented in Table 1.

From the example shown it is evident that hard source excitation (black solid line) does not give an exact correlation with the analytical modal frequencies as the soft and transparent source excitation cases do. Note that changing the receiver position does not influence the resulting frequency shift, rather, as might be expected, it changes the relative amplitudes of the resonant peaks. However, changing the source position does vary the output considerably, and this is demonstrated in Fig. 5b where the input position has been changed to (1.5, 2.0) and output point is maintained at (4.5, 3.0). In this case there is a significant shift in the frequency of the first two resonant modes (of the order of 4%), but this relative shift is not evident for the other modal frequencies presented.

This shows that the fixed grid point introduced when implementing hard source excitation not only introduces additional reflections, as identified in [10], but is also now evident as a perturbation in the resulting simulated acoustic field. The consequence is that a new set of perfectly reflecting boundary conditions are introduced in the neighborhood of the fixed point, determined by the spatial sampling interval, such that the original conditions, and hence solutions, for the otherwise empty space no longer hold in this region [20]. This results in frequency shifting of expected resonant modes. Such shifts have also been identified when single, small rigid obstacles that result in volume exclusion and wave scattering effects have been introduced into real-world rectangular acoustic chambers [19].

Soft and transparent source excitations give equivalent results in terms of frequency, that are in agreement with the analytical case, but not in terms of relative amplitude. The soft source results in a broadband offset in both 2-D and 3-D simulation, as already

Table 1
The first five predicted modal frequencies for a 5 × 5 m 2-D space with receiver located at (4.5, 3.0) and source at (a) (0.5, 2.0) and (b) (1.5, 2.0), with measured peak frequency values in Hz and relative magnitudes in dB, for hard, soft and transparent source excitation.

Predicted mode	(a)			(b)		
	Hard	Soft	Trans	Hard	Soft	Trans
48.5 Hz	49.1	48.8	48.8	51.5	48.8	48.8
(dB)	−17.5	−11.7	−18.1	−10.6	−4.4	−10.8
76.7 Hz	78.1	77.1	77.1	80.4	77.1	77.1
(dB)	−9.4	−3.6	−9.4	−5.5	0.0	−5.8
97.0 Hz	97.9	97.2	97.2	98.3	97.2	97.2
(dB)	−22.7	−14.8	−20.3	−18.8	−11.7	−17.2
108.5 Hz	110.4	108.7	108.7	109.7	108.7	108.7
(dB)	−7.1	−1.6	−6.9	−13.0	−8.7	−14.0
123.7 Hz	124.8	124.2	124.2	124.8	124.2	124.2
(dB)	−14.7	−7.6	−12.7	−16.0	−10.7	−15.8

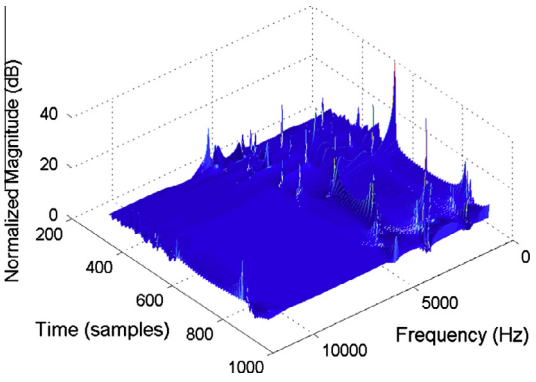

Fig. 6. Time–frequency plot of the absolute magnitude difference obtained from soft and transparent excitation under the same conditions. The soft source leads to an offset of about 4 dB across the whole spectrum for the remainder of the response after the initial wavefront has passed through the receiver point.

observed in Section 4.1, and highlighted again for the 3-D case shown in Fig. 6.

In this example, a $13.46 \times 13.46 \times 13.46$ m cubic rectilinear grid with $f_{update} = 44{,}100$ Hz, and boundaries set to be totally reflecting is defined. A source is located at the center of the grid and direct-sound only IRs obtained for distances along the 3-D diagonal axis such that dispersion error effects can be negated. For each source-receiver pairing a 1000 point impulse response is obtained (so that the effect of reflections from either the boundary or the hard source can be ignored) under hard, soft and transparent source excitation. Fig. 6 shows the waterfall plot of the absolute magnitude difference between the impulse response obtained under transparent and soft source excitation for the receiver at 2 m distance. Note that there is an overall magnitude error offset in the region of 4 dB across all frequencies after the initial wavefront has passed through the receiver point. The peaks in the response are due to the limits of numerical accuracy when performing the difference operation between the time–frequency responses for the individual IRs. When examining the difference between the transparent and hard source excitation, complete cancellation is observed verifying that the excitation methods are equivalent for this test case.

4.3. Directional source excitation

Room acoustics simulation often requires the synthesis of a directional source to simulate examples of typical real world sound sources. The excitation signals considered so far in this paper, due to the fact that they are applied at a single grid point only, have theoretically omnidirectional source behavior, limited only by the wave propagation characteristics of the FDTD grid. A number of methods have been proposed in the literature to simulate the directional characteristics of a particular radiating object (see e.g. [21,22]) but the approach considered here is that presented in [23]. This method allows simple first-order microphone-like

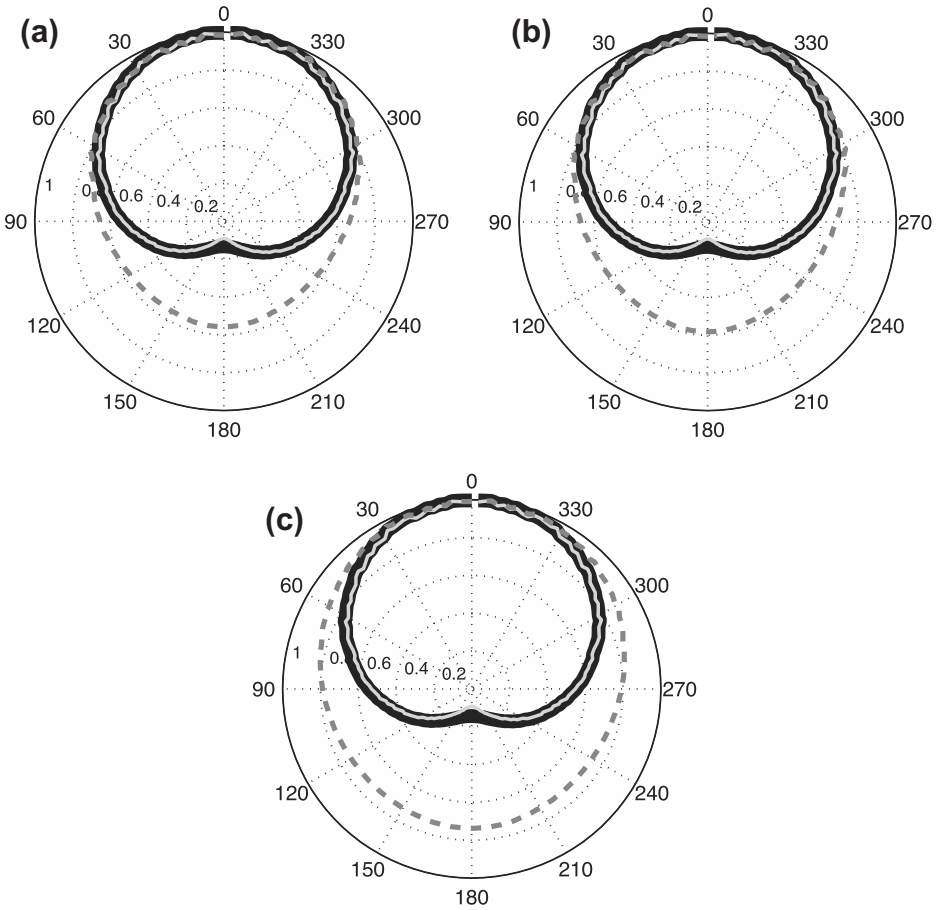

Fig. 7. Normalized 1 kHz octave bandwidth polar directivity plot, at 0.4 m from a directional source obtained from two delayed and weighted monopole omnidirectional point source excitations. The solid black and gray lines are the results obtained for the soft and transparent source cases respectively, both of which have the required cardioid directivity pattern. The dashed dark gray line is that obtained from the hard source excitation case. (a) Polar plot obtained from excitation points separated by two grid spacings, (b) four grid spacings and (c) six grid spacings.

directivity to be simulated through the use of two time-delayed, weighted and summed omnidirectional point sources. Note that all of these methods rely on correct wave interference effects to obtain the desired directional wavefront.

Two monopole sources of opposite polarity are defined in the center of a 2-D 2000×2000 point rectilinear grid, with $f_{update} = 352,800$ Hz (to ensure dispersion error is minimized in the obtained directional plots). The boundaries do not contribute to the IR at the given measurement locations and so can be considered as totally absorbing. A cardioid source directivity pattern is required in this test case, which can be obtained by defining an appropriate fractional delay between the two excitation times according to the method used in [23].

Three tests are carried out with different spacings between the two excitation points, to ensure that the results are not influenced by the effective sampling density of the FDTD grid. These correspond to two grid spacings (the excitation points are separated by one grid point), four grid spacings (points are separated by three grid points) and six grid spacings (five grid points). Hence the time delays are 2.8284 samples, 5.6568 samples and 8.4852 samples respectively. An even number of grid spacings is used in each case so that the directional source can be located and defined by a single, central grid point. An array of 180 receivers is defined at a radial distance of 0.4 m (291 axial grid points) away from the central grid location between the two sources and the direct sound from the source is captured at each and windowed appropriately. This source directivity test is repeated for hard, soft and transparent source excitation, and the resulting polar directivity plot for the octave bandwidth centered at 1 kHz is obtained as shown in Fig. 7.

Note that from Fig. 7, the hard source excitation (dashed dark gray line) does not result in the required cardioid directivity plot in any of the three grid spacing cases used, but there is good agreement between transparent (solid gray line) and soft (solid black line) sources in all examples. This implies that the increased spacing between excitation points – or equivalently, a less dense grid – has no influence on the phase cancellation required to obtain the desired directivity and is related only to the nature of the source excitation. By increasing the grid spacing further the polar response obtained tends more towards the directivity characteristics of two omnidirectional sources, noting also that this method for obtaining a directional source is dependent as much as is possible on the coincident nature of the two excitation points.

Note further that the results obtained across excitation type are not dependent on frequency, and this is in part illustrated here by considering the 1 kHz octave band, rather than considering results at a single frequency. This directional source technique is however limited by dispersion error at high frequencies, and excitation point separation at low frequencies [23]. The transparent and soft source cases are consistently accurate across the whole frequency bandwidth considered and presented in these results, and in fact the transparent source case gives slightly better cancellation at the 180° null point of the cardioid response. Ideal cancellation is noted for single frequency values when the transparent case has been considered previously [23].

5. Conclusions

This paper has discussed issues relating to source excitation in 2-D and 3-D FDTD room acoustics simulation, especially when considering impulse response measurement at single or across multiple grid points for the purposes of auralization. In particular the use of hard, soft and transparent source excitation have been considered. It has been shown that double precision calculation is a key factor in miminizing finite precision numerical effects when obtaining an IR for convolution with an arbitrary audio input and important for maintaining a sufficiently low noise floor. This might be a limiting factor for certain implementations where memory use is more critical (e.g. large, and/or real-time simulations with direct application of an input signal on a GPU),

Unit impulse excitation is the shortest possible signal that can be applied as an input, with the advantage being that no further pre-conditioning for particular circumstances or requirements is required. Any such filtering that might be needed can therefore be carried out on the IR signal obtained as the output from the system post-simulation. Unit impulse excitation also helps to minimize total computation time, noting also that the use of finite duration pulse-like signals (e.g. Gaussian, Ricker-wavelet) does not increase total computation time significantly compared with other factors such as increased spatial sampling or the problem domain size. In addition, application of a unit impulse also makes it easier to obtain and apply the compensation signal $h^n_{2D/3D}$ required to implement a transparent source. These compensation signals have been defined and presented for the particular scheme used in this paper, noting that this approach can be generalized to any other scheme as required.

Although it has been shown in previous work that fixed grid points, as used with hard source excitation, can result in additional reflections being added to the overall result, this paper has raised the additional issue of frequency shifts in the observed modal response due to the perturbation in the simulated acoustic field introduced by the hard source. The transparent source has been verified as demonstrating the benefits of the hard source excitation, in that it correctly couples the excitation signal to the grid without the introduction of additional reflections or modal shifting. Furthermore it offers improvements over soft source excitation in that it does not result in an additional broadband offset in the obtained IRs. The use of unit impulse excitation implies that post-simulation filtering can easily condition the IR for particular situations, for instance to remove the effects of the solution growth problem as demonstrated in some of the examples presented, assuming that the numerical ceiling has not been reached that would otherwise result in clipping of the output signal. Finally, a simple directional source model has been implemented that is dependent on transparent excitation given that it relies on accurately timed wave interference effects obtained via two time-delayed, weighted and summed omnidirectional point sources.

Ultimately, the final choice of excitation signal will be dependent on the application, and post-filtering might not always be desirable or optimal. For instance, if there are many receiver points, pre-filtering the *unit impulse* excitation to remove DC will deal with the solution growth problem and still deliver an output demonstrating a flat frequency response over the required audio bandwidth, removing the need for individual post-processing of each output signal. However, with multiple source points, as used here in the directional source model, and fewer receivers, post-processing would be the best choice. IR convolution with an arbitrary audio signal will also effectively remove the DC component, but windowing might be required to remove any truncation artefacts. In the best case scenario, no filtering should have to be applied either before or after simulation, with the IR obtained being the true system response appropriate for auralization or further analysis. It is with this goal in mind that this paper has explored some of the practical issues around source excitation and obtaining IRs in FDTD based room acoustics simulation. Again it is noted that each of these source models have different physical interpretations, and as a consequence, demonstrate different characteristics. Any of them might be used, if the consequences are well understood, and taken account of as appropriate. However, for room acoustics simulation the hard source is the least favorable, despite its relative simplicity, due to the fundamental changes it imparts on the underlying geometry. Future work will develop further this

transparent excitation directional source approach with a view to implementing arbitrary sound source directivities.

Acknowledgment

This work has been supported in part by the UK Engineering and Physical Sciences Research Council (EPSRC), Grants EP/F013078/1 and EP/J000108/1, and the UK Royal Academy of Engineering Grant ITG 09-373.

References

[1] Van Duyne S, Smith JO. Physical modeling with the 2-D digital waveguide mesh. In: Proceedings of the international computer music conference, Tokyo, Japan; September 1993. p. 40–7.
[2] Botteldooren D. Finite difference time domain simulation of low frequency room acoustic problems. J Acoust Soc Am 1995;98(6):33023308.
[3] Murphy D, Kelloniemi A, Mullen J, Shelley S. Acoustic modeling using the digital waveguide mesh. IEEE Signal Process Mag 2007;24:55–66.
[4] Kowalczyk K, van Walstijn M. Modelling frequency-dependent boundaries as digital impedance filters in FDTD and K-DWM room acoustics simulations. J Audio Eng Soc 2008;56:569–83.
[5] Kowalczyk K, van Walstijn M, Murphy D. A phase grating approach to modeling surface diffusion in FDTD room acoustics simulations. IEEE Trans Audio, Speech, Language Process 2011;19:528–37.
[6] Sheaffer J, van Walstijn M, Fazenda B. A physically-constrained source model for FDTD acoustic simulation. In: Proc. 15th international conference on digital audio effects (DAFx-12), York, UK, September 17–21; 2012. p. 85–92.
[7] Sheaffer J, van Walstijn M, Fazenda B. Physical and numerical constraints in source modeling for finite difference simulation of room acoustics. J Acoust Soc Am 2014;135:251–61.
[8] Karjalainen M, Erkut C. Digital waveguides versus finite difference structures: equivalence and mixed modeling. EURASIP J Appl Signal Process 2004;7:978–89.
[9] Botts J, Savioja L. Integrating finite difference schemes for scalar and vector wave equations. In: Proc. IEEE international conf. acoust., speech, signal processing. Canada (BC): Vancouver; May 2013.
[10] Schneider J, Wagner C, Ramahi O. Implementation of transparent sources embedded in acoustic finite-difference time-domain grids. J Acoust Soc Am 1998;103:136–42.
[11] Jeong H, Lam Y W. Source implementation to eliminate low-frequency artefacts in finite difference time domain room acoustic simulation. J Acoust Soc Am 2012;131:258–68.
[12] Kowalczyk K, van Walstijn M. Room acoustics simulation using 3-D compact explicit FDTD schemes. IEEE Trans Audio, Speech Language Process 2011;19:34–46.
[13] Savioja L, Välimäki V. Reducing the dispersion error in the digital waveguide mesh using interpolation and frequency-warping techniques. IEEE Trans Speech Audio Process 2000;8:184–94.
[14] Savioja L. Real-time 3D finite-difference time-domain simulation of low- and mid-frequency room acoustics. In: Proc. international conference on digital audio effects (DAFx-10), Graz, Austria; September 2010. p. 43–50.
[15] Southern A, Murphy D, Campos G, Dias, P. Finite difference room acoustic modelling on a general purpose graphics processing unit. In: Proc. of the 128th AES convention, London, UK; May 2010.
[16] López JJ, Carnicero D, Ferrando N, Escolano J. Parallelization of the finite-difference time-domain method for room acoustics modelling based on CUDA. Math Comput Modell. ISSN 0895-7177, 10.1016/j.mcm.2011.11.075. <http://www.sciencedirect.com/science/article/pii/S0895717711007606>; 2011 [available 14.12.2011].
[17] Webb C, Bilbao S. Binaural simulations using audio rate FDTD schemes and CUDA. In: Proceedings of the 15th international conference on digital audio effects (DAFx-12), York, UK, September 17–21; 2012. p. 97–100.
[18] Chen Z, Maher R. Analytical expression for impulse response between two nodes in 2-D rectangular digital waveguide mesh. IEEE Signal Process Lett 2008;15:221–4.
[19] Leung E, Lee CP, Jacobi N, Wang TG. Resonance frequency shift of an acoustic chamber containing a rigid sphere. J Acoust Soc Am 1982;72:615–20.
[20] Mehl JB, Hill RN. Acoustic eigenfrequencies of cavities with an internal obstacle: a modified perturbation theory. J Acoust Soc Am 1989;85:1841–51.
[21] Escolano J, López J, Puco B. Directive sources in acoustic discrete-time domain simulations based on directivity diagrams. J Acoust Soc Am 2007;121:EL256–62.
[22] Hacıhabiboğlu H, Günel B, Kondoz A. Time-domain simulation of directive sources in 3-D digital waveguide mesh-based acoustical models. IEEE Trans Audio, Speech Language Process 2008;16(5):934–46.
[23] Southern A, Murphy DT. Low complexity directional sound sources for finite difference time domain room acoustic models. In: Proc. of the 126th AES convention, Munich, Germany; May 2009.